Bond characteristics between high/ultra-high strength steel and ultra-high modulus CFRP laminates

Amraei Mohsen, Zhao Xiao-Ling, Björk Timo, Heidarpour Amin

DOI: 10.1016/j.engstruct.2019.110094

Contents lists available at ScienceDirect

Engineering Structures

journal homepage: http://ees.elsevier.com

Bond characteristics between high/ultra-high strength steel and ultra-high modulus CFRP laminates

Mohsen Amraei [a,b], Xiao-Ling Zhao [a,*], Timo Björk [b], Amin Heidarpour [c]

[a] The School of Civil and Environmental Engineering, UNSW Sydney, NSW 2052, Australia
[b] Laboratory of Steel Structures, LUT University, P.O. Box 20, 53851 Lappeenranta, Finland
[c] Department of Civil Engineering, Monash University, Melbourne, VIC 3800, Australia

ARTICLE INFO

Keywords
Bond
Carbon fibre reinforced polymer (CFRP)
High strength steel (HSS)
Ultra-high strength steel (UHSS)

ABSTRACT

With the increasing applications of high and ultra-high strength steel (HSS/UHSS) in engineering structures, there is a need to address rehabilitation and strengthening of such steel grades using carbon fibre reinforced polymer (CFRP). The bond between HSS/UHSS and CFRP is vital to ensure the efficiency of the strengthening. The existing bond study was focused on mild steel as substrate, with very limited work on HSS up to the grade of S690. Since HSS/UHSSs are designed to undergo much higher loading in service, much higher shear stress is expected in the adhesive layer, leading to a higher chance of premature debonding. In this paper, the bond between HSS/UHSS plates and ultra-high modulus (UHM) CFRP laminates under static tensile loading is studied experimentally, numerically and theoretically. Both single-sided and double-sided schemes were adopted. The numerical simulation using LS-DYNA software package was implemented and a reasonable agreement with the experimental results is found. A theoretical bond model was developed to relate the bond strength to the imposed strain in the steel member outside the bonded region.

1. Introduction

Carbon fiber reinforced polymers (CFRPs) which are being widely used to strengthen concrete structures for decades [1], have also recently found their way to be used as a strengthening method for metallic structures [2,3]. Significant results have been achieved in retrofitting bridge structures [4–7]. Other examples that CFRPs were used to rehabilitate metallic structures are flexural strengthening of beams made of mild steel [8–10], cracked steel plates under mix-mode fatigue loading [11], welded plates under biaxial loading [12] and welded hollow sections [13–15]. Among their desirable characteristics, light weight, availability in wide range of strength and Young's modulus, high corrosion and fatigue resistance are few to mention [16]. The current research on strengthening of steel structures using CFRPs is focused on mild steel with a very limited work on high strength steel (HSS) up to the grade S690 [17,18], and a single study on strengthening ultra-high strength steel (UHSS) circular hollow sections using CFRP sheets [19].

The applications of HSS and UHSS are becoming significantly attractive in variety of engineering sectors such as bridge construction [20], building structures [21], offshore [22] etc. With the increasing interest to use HSS/UHSS, rehabilitation and strengthening of structures made of such steel grades especially at the welded area becomes vital. Due to the very fine microstructure of these steel grades, welding an extra plate or other heat based treatments can cause further problems including fatigue cracking and strength reduction due to the softening at the weld heat affected zone (HAZ), i.e. in direct quenched UHSS [23,24]. The other method that can potentially be considered to strengthen structures made of higher grades of steel is the application of bonded CFRPs.

To enable the proper use of CFRP composites for strengthening steel structures, an understanding of bonding mechanism is therefore essential [25]. This necessity is much highlighted if CFRP is going to be used for strengthening HSS/UHSS since these steel grades undergo much higher loading, which ultimately results in higher shear stress in the bond interface. Accordingly, the chance of premature debonding and risk of failure is much higher, compared to mild and lower grades of steel [17]. Moreover, the available research in the literature on bond between CFRP and steel is mostly focused on normal modulus laminates (whereas the modulus of elasticity is mostly lower than 210 GPa) [26], low and high modulus sheets (with elastic modulus up to 640 GPa) [27,28]. There is limited research in which ultra-high modulus (UHM) CFRP laminates (with elastic modulus over 400 GPa) are used to strengthen steel structures [29,30]. The application of such CFRP laminates has the advantage of increasing both strength and stiff-

* Corresponding author.
E-mail address: xiaolin.zhao@unsw.edu.au (X-L Zhao)

https://doi.org/10.1016/j.engstruct.2019.110094
Received 1 October 2019; Received in revised form 12 December 2019; Accepted 12 December 2019
Available online xxx
0141-0296/

ness of steel members, which can potentially lead to much efficient strengthening plan [30].

This paper aims to fill the gap of knowledge in bond behavior between HSS/UHSS and UHM CFRPs. It is specifically of the notion of the authors to find out whether it is feasible to apply UHM CFRPs as a solution to strengthen structural components made of HSS/UHSS. For this aim, a series of experimental tests on the adhesively bonded UHM CFRP laminates to HSS/UHSS substrates is performed. To study the bond between steel and CFRP, four different testing set ups can be considered [16]. In this study, loading is directly applied to the steel element without any gap in both single-side and double-side bonding (SSB and DSB, respectively) schemes. In order to have a better understanding of the bonding mechanism, finite element (FE) modelling using LS-DYNA software package is implemented. Moreover, the available theoretical model by Hart Smith's [31] is implemented and it is shown that the bond strength is dependent to the imposed strain in the steel member outside the bonded region. Accordingly, for higher grades of steel, higher debonding load is expected.

2. Experimental program

2.1. Materials

Three different steel plates (i.e. S700, S960 and S1100) were chosen to study the bond between HSS/UHSS and UHM CFRP plate under quasi-static loading. Table 1 shows the nominal chemical composition of the as-received HSS/UHSS base materials (BMs).

Scanning electron microscopy (SEM) of the microstructure of BMs in this study is shown in Fig. 1. As can be seen, all the three steel grades have a mixture of bainite (B) and martensite (M). More about details of the microstructure of BMs can be found in [23]. Due to their microstructure, these grades of steel are more sensitive to welding heat input compared to lower grades of steel.

The CFRP plates were cut from pre-cured unidirectional UHM laminates with nominal thickness and width of 2.27 and 50 mm, respectively. According to the manufacturer, the CFRP laminates have Young's modulus, tensile strength and fibre content of 450 GPa, 1500 MPa and 70%, respectively. According to Ghafoori and Motavalli [30], in a study on similar CFRP from the same manufacturer, the aforementioned Young's modulus is only achieved at strain values over 0.002 mm/mm. In their study, the Young's modulus of this CFRP was calculated as 399 GPa [30].

A two part adhesive, Araldite 420 A/B is used to bond the steel substrates and CFRP laminates together. According to Fawzia [32], shear strength and tensile modulus of the adhesive are 28.6 and 1901 MPa, respectively.

2.2. Fabrication

The steel plates were first laser cut in rolling direction to the desired dimension as shown in Fig. 2. This geometry was used for tensile testing of both the steel substrates, and the bonded composite system. In the case of SSB and DSB specimens, 330 mm of the gauge length was covered with UHM CFRP.

Since the chemical bond between steel substrate and CFRP is the most important factor affecting efficiency of the adhesively bonded configurations [33], a careful attention was paid to the surface preparation during the composite system fabrication. Thus, most of the recommendations in the literature to obtain sufficient bonding strength during the preparation procedure were taken into account [11].

First, the surface of steel at the bonding region was sand blasted. This helps to increase the surface roughness, thus a better interlocking between the CFRP laminate and the steel plate. Second, the sand blasted region was cleaned using Acetone solvent. Third, the two parts of the adhesive were mixed according to the manufacturer's guideline to receive a homogeneous mixture. Fourth, a uniform adhesive layer was applied on the surface of the steel substrate immediately after surface cleaning. Fifth, the peel-ply on the surface of CFRP was removed and the surface was cleaned using Acetone solvent. Sixth, the CFRP plate was placed on the bonded region and a uniform pressure was applied on the entire surface. The composite system was clamped to ensure that excessive adhesive and air voids are squeezed out. The thickness of the adhesive was controlled at 0.4 mm based on the recommendations in the literature [26].

The bonded composite system was kept in clamped for two weeks in room temperature humidity, letting the adhesive layer to cure. In the case of DSB scheme, the preparation of the second layer followed the step-by-step procedure mentioned above. The second layer was kept in clamped for another two weeks letting the freshly bonded layer to cure. The adhesive layer thickness was measured after bonding each composite laminate to monitor if homogeneous thickness has achieved. The thickness of the adhesive layer is determined according to Eq. (1).

$$t_a = \left(t_t - t_s - t_c\right) \quad (1)$$

The terms t_a, t_t, t_s, and t_c stand for the thickness of adhesive layer, the composite system after bonding each layer, steel and CFRP, respectively. For thickness calculation of the second adhesive layer, the to-

Table 1
The nominal chemical composition of the BMs (wt.%).

Steel	C	Si	Mn	P	S	V	Cu	Cr	Ni	Mo	CEV
S700	0.12	0.25	2.10	0.020	0.10	0.20	–	–	–	–	0.38
S960	0.088	0.04	1.13	0.010	0.000	0.009	0.011	1.00	0.05	0.117	0.59
S1100	0.133	0.192	1.49	0.006	0.001	0.152	0.437	1.34	0.998	0.388	0.85

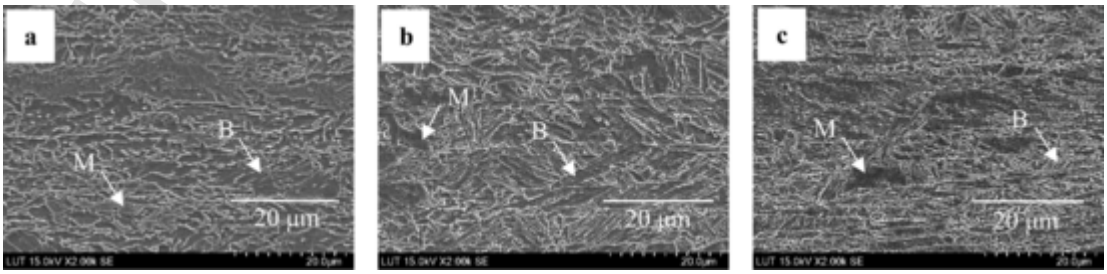

Fig. 1. SEM images of the microstructure of BMs, (a) S700, (b) S960 and (C) S1100 [23].

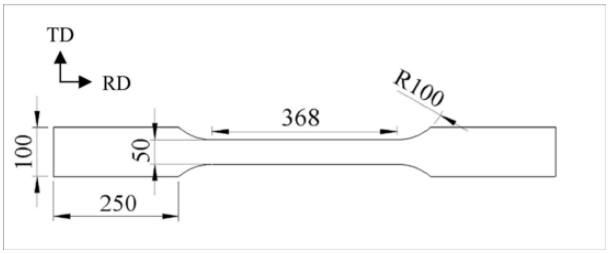

Fig. 2. Schematic of the laser cut steel specimen, TD and RD stand for transverse and rolling directions of the original steel plate, respectively. (Dimension in mm, not to scale).

tal thickness of the first layer ($t_s + t_1 + t_c$) was deducted from the total thickness of the composite system after bonding both of the layers. Table 2 shows the measured thicknesses for all specimens. The specimens were labelled as BM, SSB and DSB, which they stand for base material only, single-side bonded, and double-side bonded configurations, respectively. The letter "S" and the number in front of it represent the steel's grade.

2.3. Testing

In order to determine the mechanical properties of steel substrates, standard quasi-static tensile tests were carried out in a 1200 kN tensile testing machine with displacement control at the constant strain rate of 4×10^{-5} s^{-1}. An optical measurement device (ARAMIS) which works based on the digital image correlation (DIC) technique was utilized to measure strain values on the surface of CFRP and steel plates. At first, the surface of the specimen at the CFRP side was painted using a white matt color. Then, stochastic black speckles were sprayed on the white background. The two cameras of the optical measurement system were set in an inclined 45° angle towards the specimen so that they can measure strain values at the through thickness of steel substrate, the adhesive layer and the CFRP laminates. The two twelve mega pixel cameras of the DIC system were tilted to 25° with the distance of 240 mm. The working distance between cameras of the DIC system and the specimen was set to 620 mm. Fig. 3 shows the schematic of the test set up.

Table 2
Measured thicknesses of all specimens.

Specimen	t_s (mm)	t_c (mm)	t_t (mm)	*t_1 (mm)	*t_2 (mm)
S700 BM	8.02	–	–	–	–
S960 BM	8.22	–	–	–	–
S1100 BM	8.02	–	–	–	–
S700 SSB	8.03	2.27	10.72	0.42	–
S960 SSB	8.24	2.27	10.93	0.42	–
S1100 SSB	8.01	2.27	10.68	0.40	–
S700 DSB	8.02	2.27	13.41	0.44	0.41
S960 DSB	8.24	2.27	13.66	0.45	0.43
S1100 DSB	8.04	2.27	13.47	0.43	0.46

* t_1 and t_2 are the adhesive thickness of first and second layer, respectively.

3. Finite element modelling

The numerical simulation using LS-DYNA finite element (FE) analysis with explicit time integration was adopted in this paper. The FE model consists of three parts: steel substrate, adhesive layer and CFRP. An eight-node hexahedron solid element with constant stress formulation was utilized to mesh the entities. The mesh sizes on steel, adhesive and CFRP were chosen so that the elements are merged in longitudinal direction forming a tie constraint on the surfaces between adhesive and steel/CFRP. The element size for the steel, adhesive and composite layer are $2 \times 2 \times 2$, $2 \times 0.76 \times 0.4$ and $2 \times 2 \times 0.76$ (length, width, thickness, all in mm). Accordingly the steel and composite layer consist of 4 and 3 elements through their thickness. For the bond layer, only one element through thickness (0.4 mm layer) was utilized so that pure shear load is transferred. Damage criterion was used according to the parameters of material type 81 specifications in LS-DYNA software, with an elasto-visco-plastic behavior [34].

In order to define material properties for the steel substrate and the adhesive layer, the parameters were defined based on data from full field measurements (ARAMIS). Strain at rupture was calculated based on von Mises formula:

$$\varepsilon = \sqrt{2/3(\varepsilon_1{}^2 + \varepsilon_2{}^2 + \varepsilon_3{}^2)} \quad (2)$$

The terms ε_1, ε_2 and ε_3 represent principal strains of the element. When strain in loading direction reaches the predefined value, directional damage starts and continues until a tensile rupture strain is reached in either one of the two orthogonal directions. The constitu-

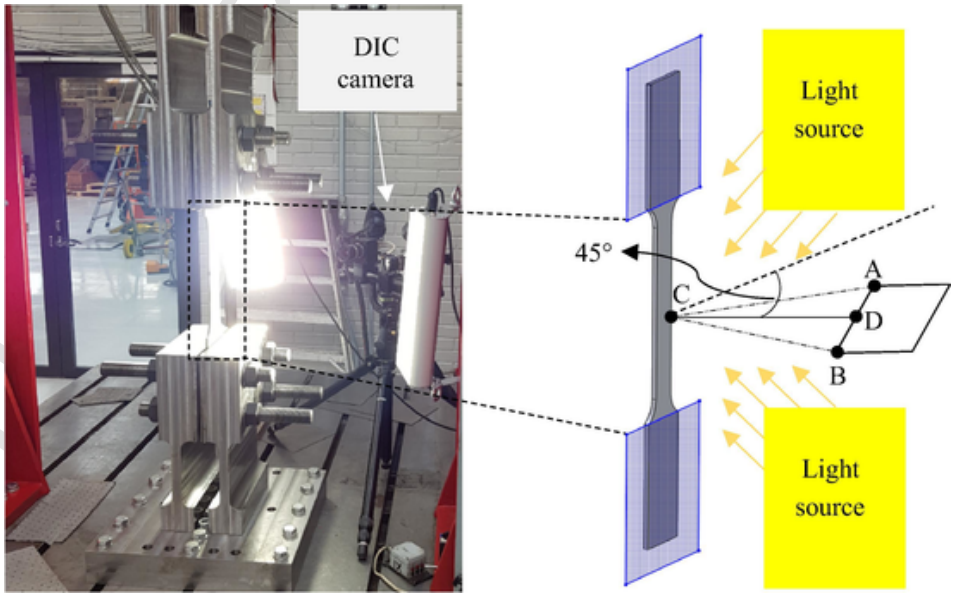

Fig. 3. Tensile test set up and position of the optical measurement system. (DIC cameras are positioned at A and B, AB = 240 mm, CD = 620 mm, ACB = 25°, not to scale).

tive properties for the damaged material are obtained from the undamaged material properties.

The damage variable (D) is defined as:

$$D = \frac{\varepsilon_p - EPPF}{EPPFR - EPPF} \quad (3)$$

where $\varepsilon_p$is the state of plastic strain, EPPF is effective plastic strain at which material softening begins, and EPPFR is the effective plastic strain at which the material ruptures. For the steel substrates, the aforementioned values are true strains calculated by the ARAMIS software from monotonic tensile tests. When the plastic strain reaches EPPFR, the element is removed from the analysis. Moreover, in order to reduce the analysis time of the FE simulation, mass scaling technique was utilized. Details of the implementation of this material model using LS-DYNA software is presented in Ref. [35].

The same procedure was applied for bonded specimens to calculate the plastic strains in the adhesive layer. The EPFF is driven from the strain reading of ARAMIS software. An elastic fully plastic behavior is considered for the adhesive layer. EPPF is considered as the maximum plastic deformation from the ARAMIS software. EPPFR is fitted value that is calculated by running the analysis of SSB specimens. When the load reaches to debonding point, the plastic strain at the element is considered as EPPFR. No damage parameter was defined for the composite material.

4. Test results

The results of the experimental program are categorized in two sub-sections including:

- BMs
- CFRP bonded specimens
  (a) SSB
  (b) DSB.

In the BM section, the tensile test results of the virgin steel plates together with FE simulations are reported. The bond test results show the tensile behavior of the bonded composite system in SSB and DSB configurations and the comparison with BM tests. Failure modes of the experimental tests are compared with the available data in the literature. Moreover, the available theoretical bond model by Hart Smith [31] for adhesively bonded composite system is validated to design against premature debonding. The test results in this paper are compared with CFRP strengthened mild steel plates.

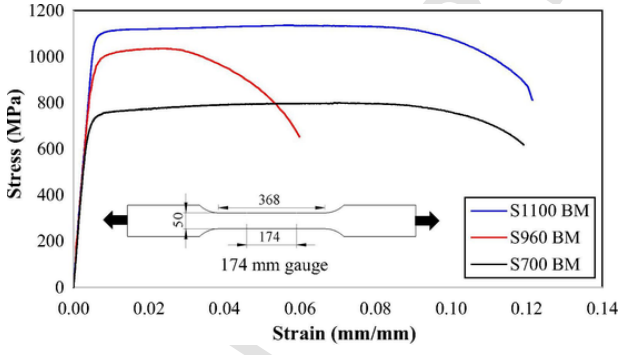

Fig. 4. The engineering stress-strain curves of the BMs (dimension in mm, not to scale).

4.1. BMs

The engineering stress-strain curves of the three steel grades are shown in Fig. 4, which were driven from consideration of 174 mm of the specimen's mid-section via the DIC system. As can be seen from Fig. 4, the S700 and S1100 which are quenched and tempered types of steel show a much ductile behavior compared to S960 which is manufactured via direct-quenching (DQ) method.

The mechanical properties of the three BMs are shown in Table 3. As can be seen from Table 3, the S1100 shows the highest ductility as $\varepsilon_u/\varepsilon_{0.2\%}$ reached 11.635, followed by S700 and S960 with measured values of 10.745 and 3.447, respectively.

At the first step for verification of FE results with the experimental tests, the tensile behavior of the BMs is simulated as explained in Section 3. Fig. 5 shows the verified load-displacement curves of S700, S960 and S1100. As can be seen from Fig. 5, he FE results show an acceptable agreement with the experimental tests.

4.2. SSB tests

Fig. 6 shows tensile test results of the SSB specimens. Debonding is noticeable as the load level in the experimental drops suddenly. As can be seen, all the specimens experienced debonding after stress reached the ultimate strength of the steel substrate outside the bonded region. Moreover, from Fig. 6 it is visible that debonding of all specimens occurs at almost similar displacement except for S1100. However, it is noticed from the experimental that the actual failure of the bond specimen occurred at lower displacement as shown using array in Fig. 6. Similar observation is visible in the FE results, which is mainly due to the higher loading rate and mass scaling in the simulation. As can be seen in Fig. 6, the S1100 SSB specimen shows a degree of end-debonding as marked via an array in Fig. 6, however, the CFRP plates was still attached to the steel substrate. As displacement increases, the adhesive layer continuously fails until the final debonding. This has resulted in a lower load drop compared to S700 and S960 SSB specimens. It is notable that no extra capacity was added to the bonded composite system compared to the BMs. The reason is that only the gauge area in the reduced cross-section was covered by CFRP.

The experimental program and bond results of SSB specimens are summarized in Table 4. F_{max} is referred to the maximum load that the composite system can carry before the adhesive layer is debonded. ε_{max} CFRP refers to the maximum strain at the CFRP when load reaches to the ultimate bond strength. F_{nom} CFRP is the maximum load that the CFRP carries which is calculated according to Eq. (4):

$$F_{nom}CFRP = (\varepsilon_{max}CFRP) \times (A_{CFRP}) \times (E_{CFRP}). \quad (4)$$

Moreover, F_S is the nominal load at the steel substrate when strain at the CFRP reaches to its maximum, which is calculated according to Eq. (5).

$$F_S = (F_{max}) - (F_{nom}CFRP) \quad (5)$$

Table 3
The mechanical properties of BMs.

Steel' grade	E (GPa)	$f_{0.2\%}$ (MPa)	f_u (MPa)	$f_u/f_{0.2\%}$	$\varepsilon_{0.2\%}$ (%)	ε_u(%)	$\varepsilon_u/\varepsilon_{0.2\%}$	A_5 (%)
S700	196	735	798	1.086	0.580	6.232	10.745	11.91
S960	197	987	1035	1.049	0.707	2.437	3.447	5.98
S1100	201	1106	1136	1.027	0.501	5.829	11.635	12.16

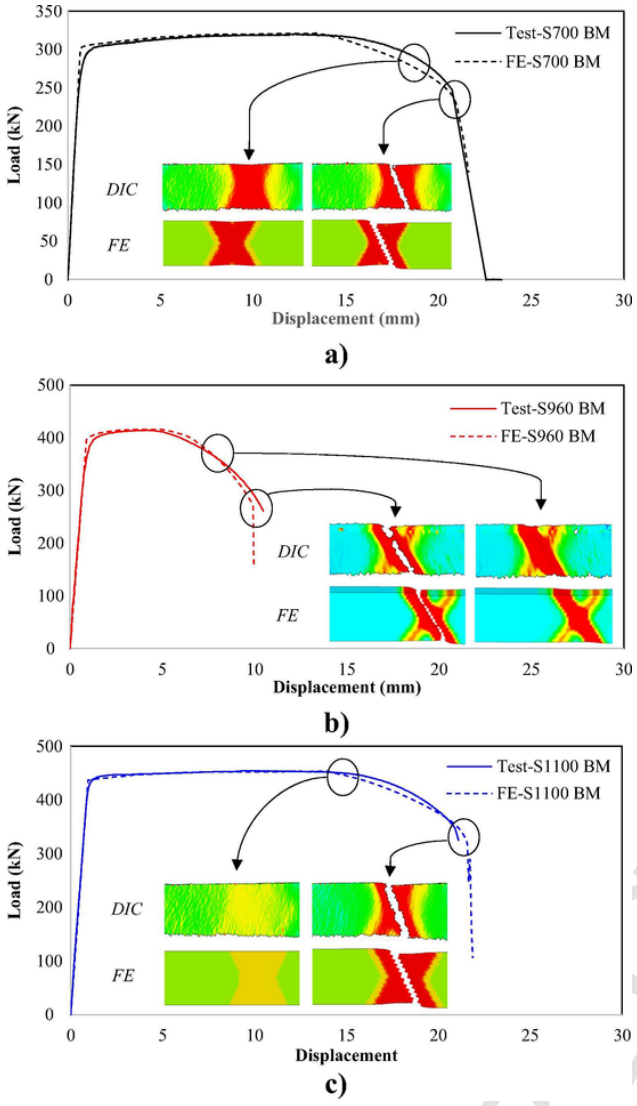

Fig. 5. Comparison of load-displacement curves of the BMs from experimental testing and FE modelling, (a) S700, (b) S960 and (c) S1100.

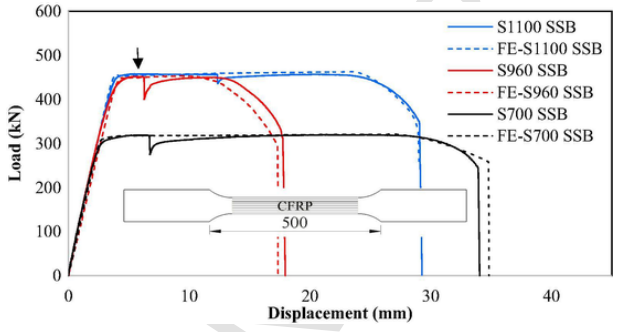

Fig. 6. Tensile test results of the SSB specimens.

The term "f_s nom" is referred to the nominal stress in steel substrate calculated from Eq. (5) with respect to the specimen's dimension. The term "f_s max" is the maximum stress in steel substrate at the un-strengthened side. The terms "T" and "FE" stand for experimental testing and finite element, respectively. Since the strength and thickness of the adhesive layer is much lower than the steel substrate and CFRP laminates, the load carrying capacity of the bond layer has not been considered for these calculations.

According to Table 4, the maximum stress in the steel substrate at the un-strengthened side (middle of the specimen) is still lower than the yield strength of the steel plate even the applied loading is at the ultimate strength of the BM. This shows the effectiveness of CFRP strengthening to reduce stress in HSS/UHSS. However, excessive interfacial shear stress at the bond line due to steel's yielding was reported when dogbone specimens made of mid steel plates were strengthened using UHM CFRP [36]. Even though they only used DSB specimens, yet the yielding of steel at the neck area of specimen caused higher shear stress in the adhesive layer, hence failure of the specimen [36].

From Table 4 it is also understood that the minimum debonding load, which belongs to S700 SSB, is 318.3 kN. The equivalent bond strength per unit width of this specimen is 6.36 kN/mm. This bond strength is three times higher compared to mild steel plates with thickness of 6 mm strengthened with normal modulus CFRP in DSB configuration (1.97 kN/mm) [37]. It is notable that the test configuration in [37] is similar to this paper, except that it only applies CFRP laminates in DSB configuration. The minimum bond strength of SSB specimen in this study is equivalent to the mild steel specimen strengthened with similar UHM CFRP in DSB configuration [36]. This implies the efficiency of strengthening HSS/UHSS compared to lower grades of steel as the composite system undergo its maximum capacity.

Furthermore, as can be seen from Table 4, the reduction of nominal stress in cross-section of the steel plate is ranging from 28 to 34%. However, if the maximum stress in the steel plate is considered, which occurs at the mid-thickness of the steel substrate, the reduction is in the range of 18–24%. This stress reduction by the means of CFRP bonding is enough to retain the mechanical properties of UHSS steels after welding. According to Amraei et al. [35], the reduction of the ultimate strength of welded UHSS S960 after welding is 13%. Hence, the bonded CFRP can potentially strengthen welded UHSS under static loading using SSB configuration. Further experimental tests are needed to identify the effectiveness of CFRP strengthening for welded HSS/UHSS.

According to the classification proposed by Zhao and Zhang [16], six possible failure modes between CFRP and steel include: (a) steel and adhesive interface failure; (b) cohesive failure (adhesive layer failure); (c) CFRP and adhesive interface failure; (d) CFRP delamination; (e) CFRP rupture; (f) steel yielding.

For the SSB specimens, the major failure mode was end debonding due to adhesive layer failure, interface debonding between adhesive and steel/CFRP (mode a, b and c). However, CFRP and adhesive interface debonding (mode c) was dominant throughout the specimen (apart from the end debonding), as shown in Figs. 7–9. According to Table 4, although the steel plates experience yielding outside the bonded region, no steel yielding has happened in the bonded region for the steel grade and thickness range in this test program.

The failure mode in the current study is different compared with the bonded UHM CFRP plates to mild steel when Araldite adhesive is used. According to [29], CFRP rupture (mode e) is dominant when double strap joints were tested if bond length exceeds the effective bond length. However, CFRP delamination (mode d) occurs if bond length is smaller than the effective bond length. CFRP rupture was also reported when UHM CFRP was used to strengthen dogbone shape mild steel plates in tensile mode [36]. For bonded CFRP laminates with elastic modulus of 165 GPa to mild steel, cohesive failure (mode b) is reported [38]. However, steel and adhesive interface debonding (mode a) was dominant if the applied load is fatigue [39]. According to Hu et al. [17], premature debonding at stress range equivalent to 50% of the yield strength of S690 steel has happened when UHM CFRP sheets with thickness of 0.16 mm are used to strengthen cracked steel plates under fatigue loading. However, no premature debonding up to the ulti-

Table 4
The bond test results of SSB specimens.

Specimen	F_{max} T (kN)	F_{max} FE (kN)	ε_{max} CFRP T (%)	ε_{max} CFRP FE (%)	F_{nom} CFRP T (kN)	F_{nom} CFRP FE (kN)	Fs T (kN)	Fs FE (kN)
S700 SSB	318.3	321.1	0.32	0.31	113.3	109.8	205	211.3
S960 SSB	450.9	446.1	0.42	0.40	148.7	141.6	302.2	304.5
S1100 SSB	456.7	453.1	0.45	0.42	159.4	148.7	297.3	304.4
Specimen	f_S nom T (MPa)	f_S nom FE (MPa)	f_S max (MPa)	$f_{0.2\%}$ BM (MPa)	f_u BM (MPa)	f_S nom/f_u BM (T)	f_S nom/f_u BM (FE)	f_S max/f_u BM (FE)
S700 SSB	521	539	627	735	798	0.65	0.68	0.79
S960 SSB	744	752	845	987	1035	0.72	0.73	0.82
S1100 SSB	755	775	868	1106	1136	0.66	0.68	0.76

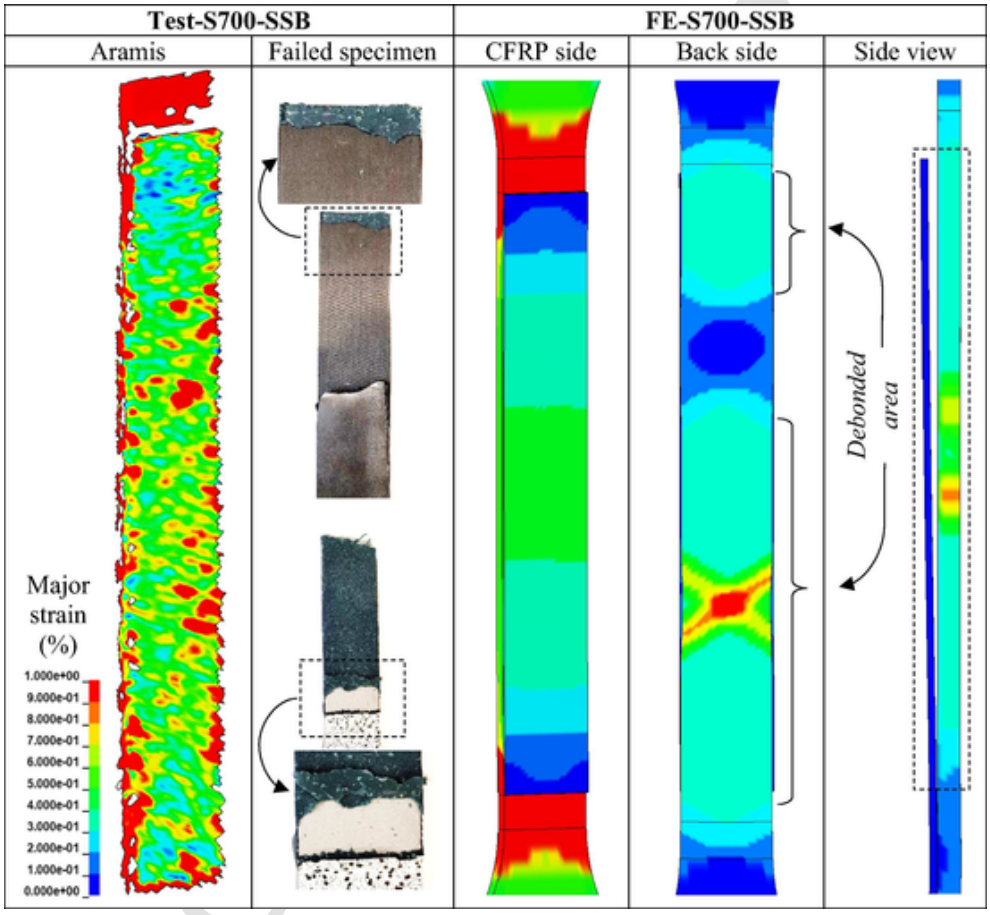

Fig. 7. Failed specimens of S700-SSB.

mate strength of all steel grades for SSB specimens in this study has been found.

In order to simulate the debonding using FE analysis, element deletion due to excessive damage is implemented. Accordingly, all the simulated SSB show adhesive layer failure with no interface debonding. Even though the failure mode is different compared to the experimental results, yet the FE analysis provided a precise indication of the debonding initiation and the strain distribution throughout the steel substrate, adhesive layer and CFRP plate. After debonding, the steel plates failed similar to BMs by forming a shear band in approximate angle of 30°.

4.3. DSB tests

Fig. 10 shows the load-displacement curves of the DSB specimens. As can be seen, no debonding has happened for all steel grades. The FE results are in agreement with the experimental tests revealing no premature debonding as shown in Fig. 10. However, excessive localized strain at the both ends resulted in local debonding predominantly by modes (a) and (b). Figs. 11–13 show the local debonding at CFRP ends.

Since no debonding has occurred for DSB specimens, F_{max} only refers to the ultimate load that the steel plate can carry. For the DSB specimens, the reduction factor by CFRP plate is considered as two

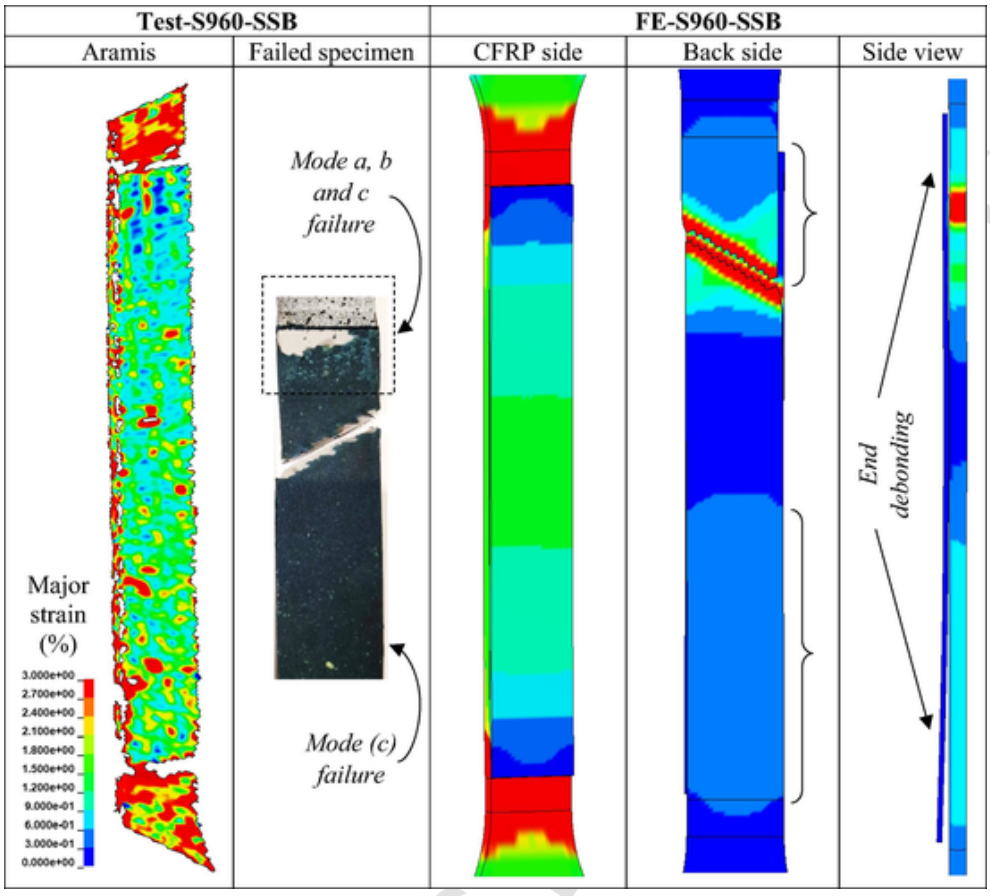

Fig. 8. Failed specimens of S960-SSB.

due to the equal contribution of the bonded composite laminates. Table 5 summarizes the experimental and numerical results of DSB specimens.

As can be seen from Table 5, all the specimens show a considerable reduction in the stress at the steel substrate in the DSB configuration. The reduction of the nominal stress in the cross-section of the steel plate is ranging from 52 to 56%. However, if the maximum stress in the steel plate is considered, which occur at the mid-thickness of the steel substrate, the reduction is in the range of 43–45%. According the current results, DSB strengthening of HSS/UHSS can potentially compensate the strength reduction due to the HAZ as reported in the literature [19,23].

By comparing the results with similar test configurations on lower grades of steel, higher debonding load can be achieved in HSS/UHSS bonded systems. According to Colombi and Poggi [37], bond strength per unit length of mild steel plates strengthened in DSB configuration using normal modulus CFRP was 1.97 kN/mm. However, the current study demonstrates that the bond strength of DSB specimens is higher than 9.13 kN/mm as no debonding has happened even for S1100 DSB. According to Al-Emrani et al. [36], bond strength of mild steel plates in DSB configuration strengthened with UHM CFRP was 6.86 kN/mm. It is notable that the whole gauge between the grips was covered with CFRP in their study. Yet, they reported yielding of steel at the neck area resulted in excessive shear stress at the adhesive interface and failure of the specimen.

5. Theoretical bond models

Fig. 14 shows the schematic of DSB specimen. The linear-elastic stress analysis for adhesively bonded strap joints is proposed by Hart-Smith's formulation [31]. Considering the approach proposed by Albat and Romilly (1999) which extends the analytical Hart-Smith's for adhesively bonded plates in which composite is attached symmetrically to the both sides of the substrate [40], shear stress at the bond interface, and stress in the composite layer follow equations (6) and (7), respectively:

$$\tau_{(x)} P\left(\frac{E_c t_c}{E_s t_s + 2E_c t_c}\right)\lambda\frac{e^{\lambda x} - e^{-\lambda x}}{e^{\lambda L} + e^{-\lambda L}} \tag{6}$$

$$\sigma_{(x)} P\left(\frac{E_c}{E_s t_s + 2E_c t_c}\right)\left(1 - \frac{e^{\lambda x} + e^{-\lambda x}}{e^{\lambda L} + e^{-\lambda L}}\right) \tag{7}$$

where P is the applied tensile load for unit width, E_c, t_c and E_s, t_s are, respectively, the Young's modulus, thickness of the CFRP strips and the steel plate. The term × is the distance from the specimen's axis until it reaches the effective bond length "L". λ is given by:

$$\lambda^2 = \frac{G_a}{t_a}\left(\frac{1}{E_c t_c} + \frac{2}{E_s t_s}\right) \tag{8}$$

where G_a and t_a are the shear modulus and thickness of the adhesive layer, respectively. Considering a normal modulus CFRP with elastic modulus of 200 GPa with the thickness of 1.4 mm being used to strengthen a 5 mm steel plate using a 0.5 mm adhesive layer, the value of lambda will be 0.0178 mm^{-1}.

According to Eq. (6), and the assumption that $e^{\lambda L} \gg 1$, $\tau_{(max)}$ occurs at x = L, hence:

$$\begin{aligned}\tau_{(max)} &= P\left(\frac{E_c t_c}{E_s t_s + 2E_c t_c}\right)\lambda\frac{e^{\lambda L} - e^{-\lambda L}}{e^{\lambda L} + e^{-\lambda L}} \\ &= P\left(\frac{E_c t_c}{E_s t_s + 2E_c t_c}\right)\lambda\end{aligned} \tag{9}$$

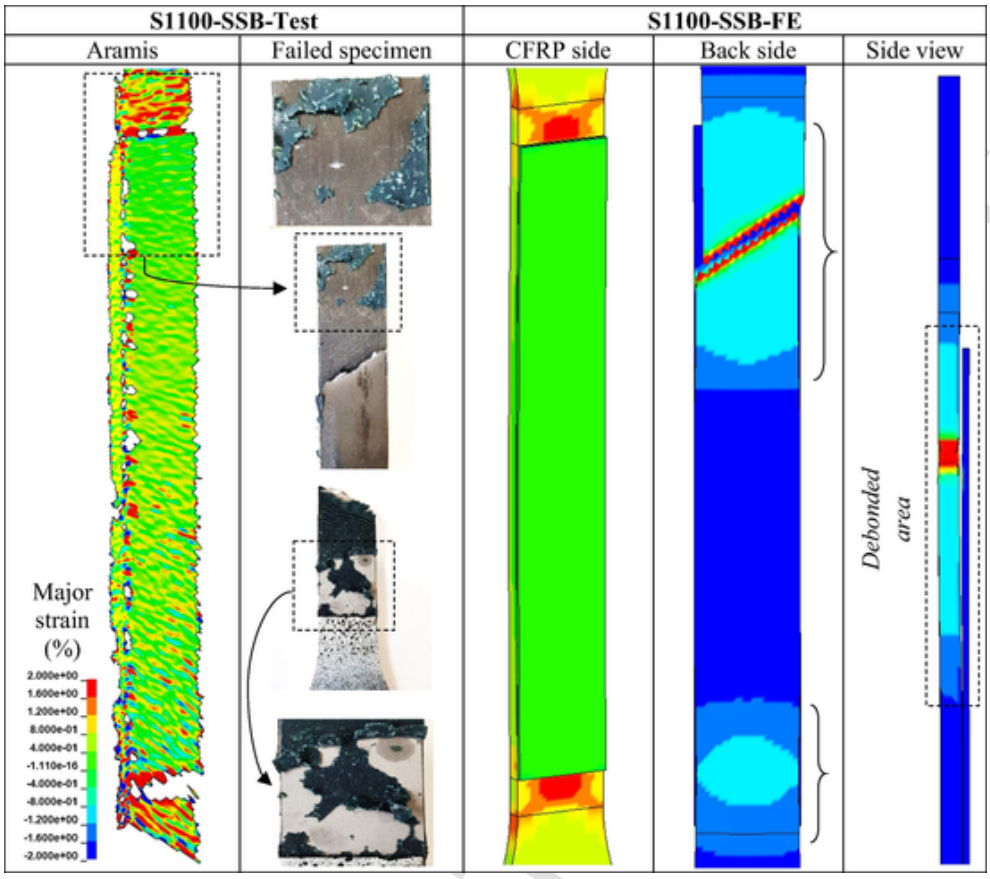

Fig. 9. Failed specimens of S1100-SSB.

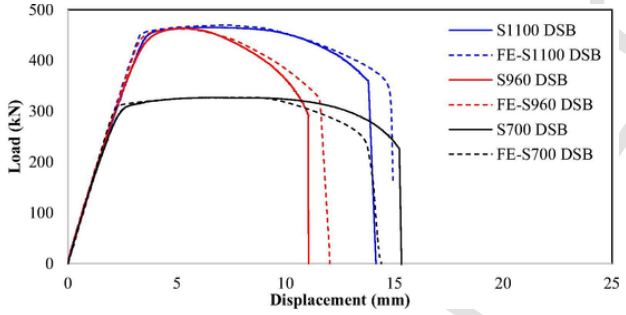

Fig. 10. Tensile test results of the DSB specimens.

$$P = \sigma_s t_s = E_s t_s \varepsilon_s \tag{10}$$

where σ_s and ε_s are referred to the maximum stress, and strain in the steel member outside the bonded region, respectively. According to equations (9) and (10),

$$\tau_{(max)} = E_s t_s \varepsilon \left(\frac{E_c t_c}{E_s t_s + 2E_c t_c} \right) \varepsilon_s \tag{11}$$

and,

$$\varepsilon_s = \left(\frac{\tau_{(max)}}{E_c} \right) \times \left(\frac{1}{\lambda t_c} \right) \left(1 + 2 \left(\frac{E_C}{E_s} \times \frac{t_c}{t_s} \right) \right) \tag{12}$$

It is notable that all terms in Eq. (12) are non-dimensional. From Eq. (7), by assuming that $e^{\lambda L}$ is much bigger that 1, the maximum stress in the CFRP laminate occurs at X = 0, hence:

$$\sigma_{(max)}CFRP = P \left(\frac{E_c}{E_s t_s + 2E_c t_c} \right) \tag{13}$$

by taking the Eq. (10) into account,

$$\sigma_{(max)}CFRP = \left(\frac{E_s t_s}{E_s t_s + 2E_c t_c} \right) E_c \varepsilon_s \tag{14}$$

and,

$$\varepsilon_{CFRP} = \left(\frac{E_s t_s}{E_s t_s + 2E_c t_c} \right) \varepsilon_s \tag{15}$$

The Eqs. (12) and (15) show that the bond strength for a given geometry and elastic modulus is dependent on the applied strain in the steel member outside the strengthened region. It is notable that the following equations are valid in the elastic regime of the adhesive layer. In the case of HSS/UHSS, since the elastic modulus is similar to mild steel, debonding should occur when strain at the steel member outside the strengthening region reaches a certain value.

According to Eq. (12), considering the mechanical properties of the materials used in this study, in order to reach the ultimate shear strength of the adhesive layer, strain values at the steel substrate outside the strengthened region should reach 0.105%. According to Table 3, the 0.2% proof strain of all the HSS/UHSS studied in this paper are above this value, hence no steel yielding occurs. This strain value at the steel plate outside the bonded region is the minimum in which shear stress at both ends of the bond reaches its maximum. The correspondent stress in the steel substrate outside the strengthened area at this strain value is 210 MPa. Consequently, the load per unit width of this stress is 1.68 kN (nominal plate thickness of 8 mm).

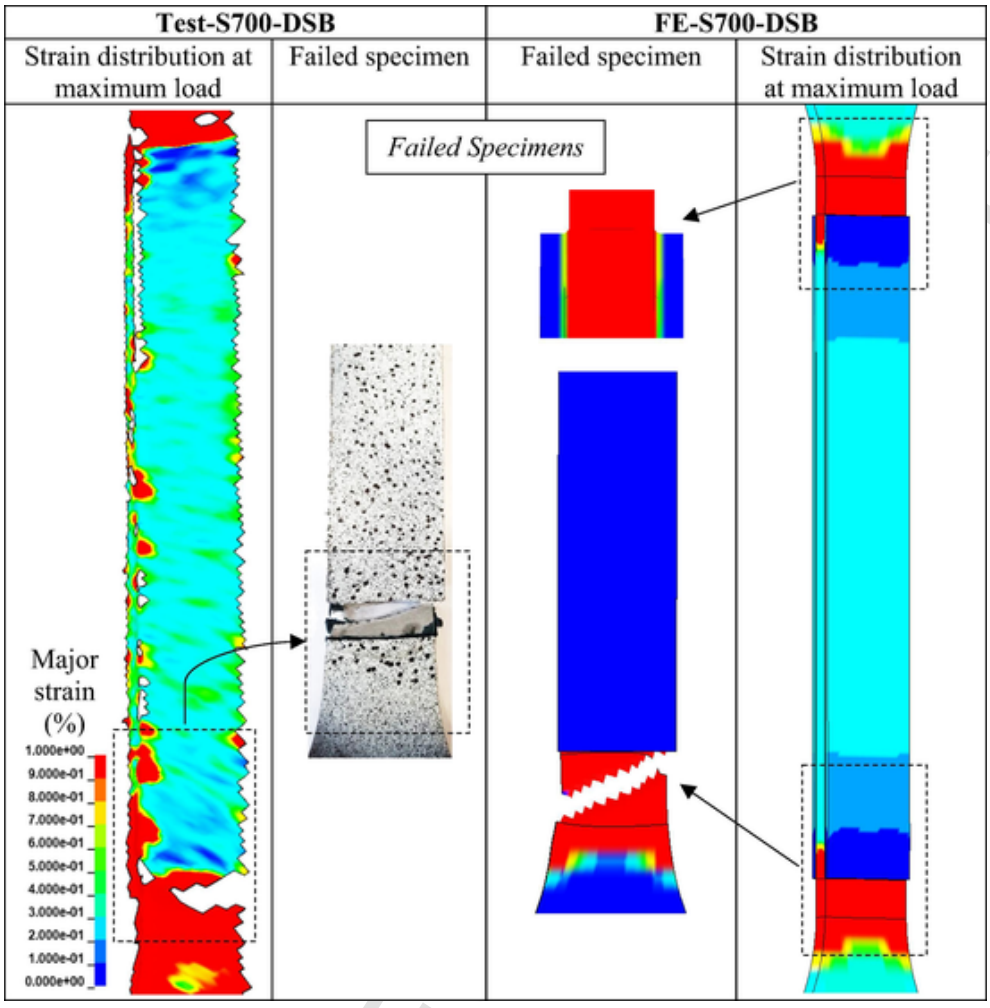

Fig. 11. Failed specimens of S700-DSB.

Assuming a bilinear bond-slip model for the CFRP-bonded to steel composite system, as proposed in the literature [16,25,27,38,41], the bond-slip model is similar to Fig. 15. Wu et al. [29], proposes the plastic shear strain (γ_p) of the adhesive to be 5 times of its elastic shear strain (γ_e) in strap joints made of steel and UHM CFRP. This proposal is due to the high strain energy capacity of Araldite 420 as reported in the literature [41]. In such a model, the required strain energy to fully debond the adhesive layer is six times of the strain energy to reach the adhesive's shear strength at the elastic region. Considering the calculated P in the elastic region of the adhesive, if steel yielding does not occur, the total force required to debond the adhesive layer is 10.08 kN/mm. This force value would result in 1260 MPa stress in the steel plate outside the strengthened region which is above the ultimate strength of all steel grades studied in this paper. Based on theoretical approach, steel rupture outside the strengthened region should govern failure of the specimens. As mentioned in Section 4.3, both experimental and FE models showed no adhesive failure for DSB specimens in this study, and steel rupture outside the strengthened region was the failure mode of DSB specimens.

However, steel yielding at the bonded area must be checked prior to considering steel rupture outside the strengthened region. The FE results show that no steel yielding at the bonded area has occurred, as shown in Section 4.3. According to [36,37], for mild steel specimens in the thickness range between 6 and 10 mm strengthened with both normal modulus and UHM CFRP laminates, in which adhesive' shear strength is similar to Araldite 420 A/B, steel yielding in the bonded region governing the failure. Due to the high strain energy capacity of mild steel, shear stress in the adhesive layer reaches its ultimate capacity throughout the entire bond area. Hence, steel yielding developed in the entire steel substrate, resulted in interfacial debonding of the adhesive and CFRP prior to rupture of the steel substrate [36,37]. Based on this observation, there is a difference in the debonding mechanism of HSS/UHSS compared to mild steel. Accordingly, higher bond strength is reachable for HSS/UHSS specimens compared to mild steel, as demonstrated in Sections 4.2 and 4.3.

Fig. 16 shows schematic of the SSB specimen. Considering similar approach for SSB specimens, the following equations could be driven:

$$\tau_{(x)} = P\left(\frac{E_c t_c}{E_s t_s + E_c t_c}\right)\lambda\frac{e^{\lambda x} - e^{-\lambda x}}{e^{\lambda L} + e^{-\lambda L}} \tag{16}$$

$$\lambda^2 = \frac{G_a}{t_a}\left(\frac{1}{E_c t_c} + \frac{1}{E_s t_s}\right) \tag{17}$$

$$\sigma_{(max)}CFRP = \left(\frac{E_s t_s}{E_s t_s + E_c t_c}\right)E_c \varepsilon_s \tag{18}$$

$$\varepsilon_s = \left(\frac{\tau_{(max)}}{E_c}\right)\times\left(\frac{1}{\lambda t_c}\right)\left(1 + \left(\frac{E_C}{E_s}\times\frac{t_c}{t_s}\right)\right) \tag{19}$$

$$\varepsilon_{CFRP} = \left(\frac{E_s t_s}{E_s t_s + E_c t_c}\right)\varepsilon_s \tag{20}$$

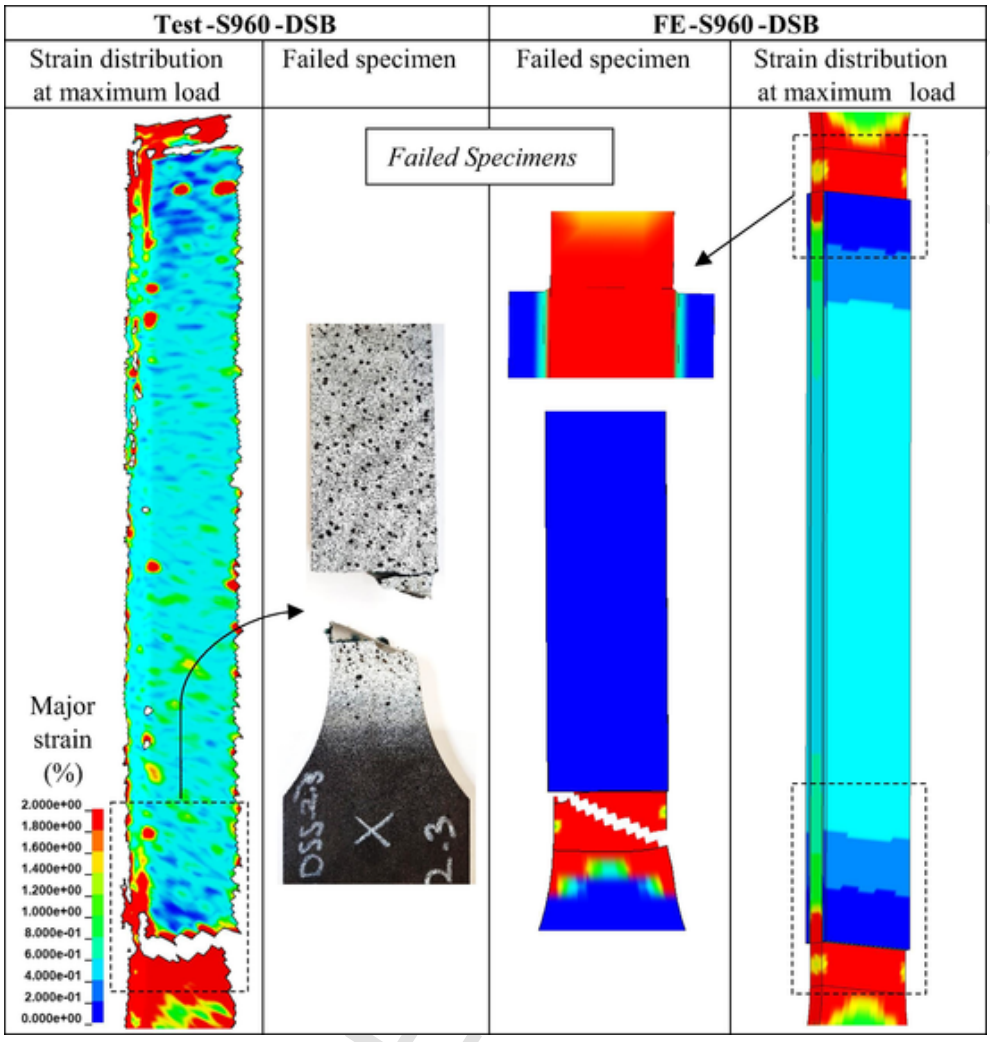

Fig. 12. Failed specimens of S960-DSB.

It is notable that eccentricity of the loading is not considered in this study since the focus is on thin steel plates with thickness of 8 mm. According to Eq. (19), ultimate shear strength of the bond would occur when strain at the steel substrate outside the bonded region reaches 0.09%. This value is below yield strength of low carbon steels. The equivalent stress in the steel substrate outside the strengthened region and the P value of this strain are 180 MPa and 1.439 kN/mm, respectively. By utilizing the strain energy approach similar to DSB specimens, the total debonding force calculates as 8.634 kN/mm. Consequently, the stress in the steel plate outside the strengthened should reach 1079.25 MPa (for 8 mm steel plate). The calculated stress is above ultimate strength of S700 and S960 steel plates. However, it is slightly below the capacity of S1100 (1136 MPa). The variation in the material properties and the assumptions used in the analytical model can affect this calculation. Yet, the analytical approach provides a reasonable agreement with the experimental and FE modelling.

6. Conclusions

This paper is dedicated to study the bond between HSS/UHSS and UHM CFRP experimentally, numerically and theoretically. For this aim, steel plates made of S700, S960 and S1100 were bonded to CFRP laminates with nominal Young's modulus of 450 GPa. Araldite adhesive was used to manufacture the composite system in SSB/DSB schemes. According to the results, following conclusions are driven:

- For SSB specimens, debonding occur after loading reached to the ultimate strength in the steel substrate outside the bonded region.
- The strain value at which debonding occurs for all SSB specimens is similar. According to the Hart smith's model, the critical strain in the steel substrate outside the bonded region, in which debonding will happen, governs. The critical strain is dependent on non-dimensional parameters such as $\frac{\tau_{(max)}}{E_c}$, $\frac{1}{\lambda t_c}$, $\frac{E_C}{E_s}$ and $\frac{t_c}{t_s}$.
- Failure mode of the SSB specimens was a combination of steel-adhesive interface failure, cohesive failure and adhesive-CFRP interface failure at the both ends of the bonded region. Apart from that area, the major failure mode was adhesive-CFRP interface failure.
- The DSB specimens experienced excessive strain at the both ends of the bonded area, however, the bond stayed intact and CFRP plates were fully in action. For the studied steel grades and thickness in this study, failure mode was steel rupture outside the strengthened region as no debonding happened.
- The failure mechanism of the studied HSS/UHSS is different compared to mild steel. By increasing the yield strength of the steel substrate, the load at which debonding occurs increases, too. Hence, efficiency of the composite system using HSS/UHSS is higher than lower grades of steel.
- The debonding load is calculated using the strain energy capacity of the adhesive layer. For Araldite 420, the total required energy is

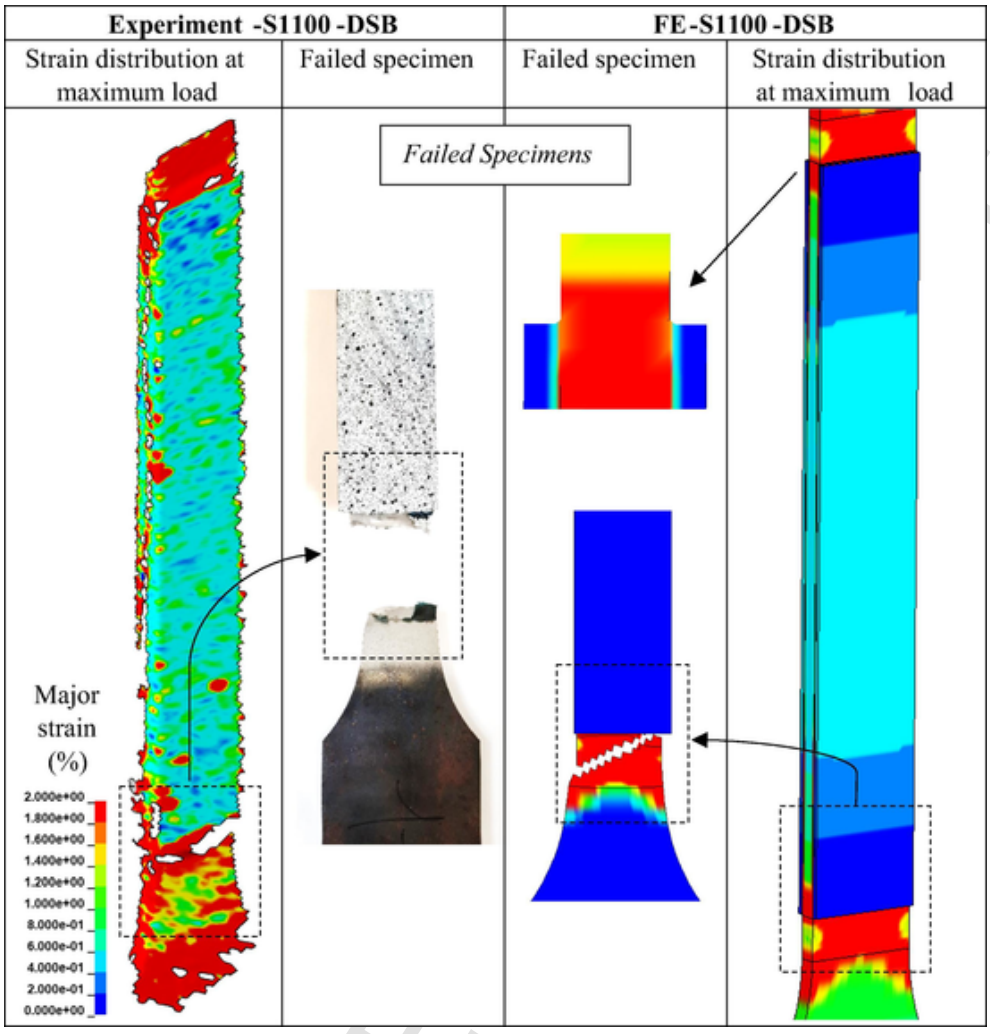

Fig. 13. Failed specimens of S1100-DSB.

Table 5
The bond test results of DSB specimens.

Specimen	F_{max} T (kN)	F_{max} FE (kN)	ε_{max} CFRP T (%)	ε_{CFRP} max FE (%)	F_{nom} CFRP T (kN)	F_{nom} CFRP FE (kN)	Fs T (kN)	Fs FE (kN)
S700 DSB	326.8	326.9	0.29	0.28	91.3	95.3	144.1	136.2
S960 DSB	464.1	462.4	0.38	0.36	119.7	122.6	224.7	217.2
S1100 DSB	465.5	469.5	0.40	0.39	126.0	132.8	213.5	203.9
Specimen	f_S nom T (MPa)	f_S nom FE (MPa)	f_S max FE (MPa)	$f_{0.2\%}$ BM (MPa)	f_u BM (MPa)	f_S nom/f_u BM (T)	f_S nom/f_u BM (FE)	f_S max/f_u BM (FE)
S700 DSB	345	340	439	735	798	0.43	0.43	0.55
S960 DSB	512	510	589	987	1035	0.49	0.49	0.57
S1100 DSB	524	543	625	1106	1136	0.46	0.48	0.55

six times higher than the required energy to reach adhesive's shear strength.

- Both SSB and DSB specimens reduced the maximum stress in the steel substrate at the bonded region by 18–24% and 43–45%, respectively. The reduction in the magnitude of stress can potentially compensate the stress reduction due to the HAZ of welded plates made of HSS/UHSS.

According to the findings of this paper, authors would suggest further research to be conducted on the strengthening of welded details made of HSS/UHSS under static and fatigue loading. It is also suggested to find out optimum thickness of steel plates to prevent fatigue failure due to debonding. Effects of environmental conditions on the durability of bond between HSS/UHSS and UHM CFRP is another topic that needs to be addressed.

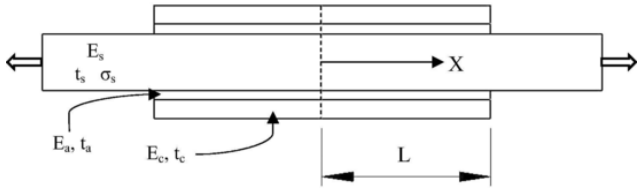

Fig. 14. Schematic of the DSB specimen.

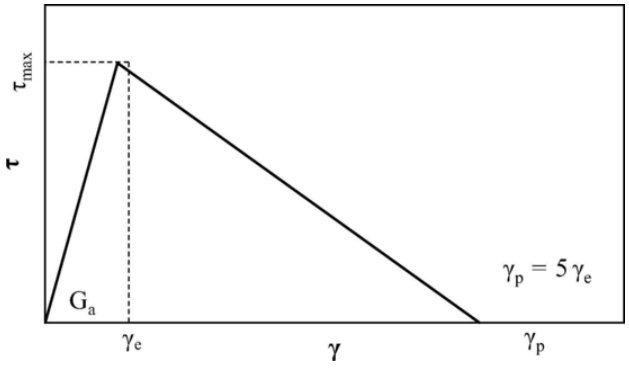

Fig. 15. Schematic of a bilinear bond-slip model for the adhesive layer.

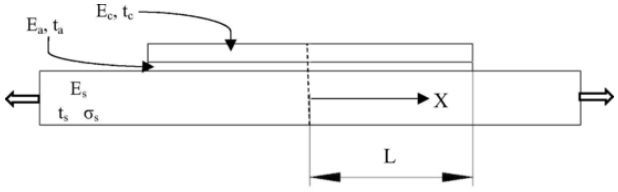

Fig. 16. Schematic of the SSB specimen.

CRediT authorship contribution statement

Mohsen Amraei: Conceptualization, Data curation, Formal analysis, Investigation, Methodology, Software, Validation, Visualization, Writing - original draft, Writing - review & editing. **Xiao-Ling Zhao:** Conceptualization, Funding acquisition, Investigation, Methodology, Project administration, Resources, Supervision, Validation, Writing - review & editing. **Timo Björk:** Funding acquisition, Resources, Supervision, Writing - review & editing. **Amin Heidarpour:** Funding acquisition, Resources, Supervision, Writing - review & editing.

Declaration of Competing Interest

The authors declared that there is no conflict of interest.

Acknowledgment

The authors wish to thanks financial support of the Business Finland through ISA-LUT project (23B256A), and the Australian Research Council through Discovery Project (DP150100442). The first author of this paper appreciates Monash University by receiving the GRITA award. The authors wish to thank SSAB Europe Co by providing the steel plates for this research. Special thanks to the technical support of the staff members at Laboratory of Steel Structures, and Laboratory of Laser Processing. The help and support of Mr. Antti Ahola, Mr. Matti Koskimäki and Mr. Olli-Pekka Pynnönen in conducting the experimental tests is greatly appreciated.

References

[1] JG Ten, JF Chen, ST Smith, L Lam. FRP—strengthened RC structures. West Sussex, UK: John Wiley and Sons Ltd; 2002.
[2] JMC Cadei, TJ Stratford, LC Hollaway, WG Duckett. Strengthening metallic structures using externally bonded fibre-reinforced composites. London: CIRIA; 2004.
[3] XL Zhao. FRP strengthened metallic structures. Boca Raton, FL, USA: CRC Press, Taylor & Francis Group; 2013.
[4] E Ghafoori, M Motavalli, A Nussbaumer, A Herwig, GS Prinz, M Fontana. Design criterion for fatigue strengthening of riveted beams in a 120-year-old railway metallic bridge using pre-stressed CFRP plates. Compos B 2015;68:1–13.
[5] E Ghafooria, A Hosseinia, R Al-Mahaidi, X-L Zhao, M Motavalli. Prestressed CFRP-strengthening and long-term wireless monitoring of an old roadway metallic bridge. Eng Struct 2018;176:585–605.
[6] TC Miller, MJ Chajes, DR Mertz, JN Hastings. Strengthening of a steel bridge girder using CFRP plates. J Bridge Eng ASCE 2001;6(6):514–522.
[7] M Tavakkolizadeh, H Saadatmanesh. Fatigue strength of steel girders strengthened with carbon fiber reinforced polymer patch. J Struct Eng 2003;129:186–196.
[8] TW Siwowski, P Siwowska. Experimental study on CFRP-strengthened steel beams. Compos B 2018;149:12–21.
[9] NK Photiou, LC Hollaway, MK Chryssanthopoulos. Strengthening of an artificially degraded steel beam utilizing a carbon/glass composite system. Constr Build Mater 2006;20(1–2):11–21.
[10] S Rizkalla, T Hassan, N Hassan. Design recommendations for the use of FRP for reinforcement and strengthening of concrete structures. Prog Struct Mat Eng 2003;5(1):16–28.
[11] NJ Aljabar, XL Zhao, R Al-Mahaidi, E Ghafoori, M Motavalli, N Powers. Effect of crack orientation on fatigue behavior of CFRP-strengthened steel plates. Compos Struct 2016;152:295–305.
[12] H Liu, X-L Zhao. Prediction of fatigue life for CFRP strengthened steel connections under combined loads. Int. J. Struct. Stab. Dyn. 2013;13(4). doi:10.1142/S0219455412500599.
[13] X-G Xiao, X-L Zhao. CFRP repaired welded thin-walled cross-beam connections subject to in-plane fatigue loading. Int J Struct Stab Dyn 2011;12(1):195–211.
[14] J Nadauld, CP Pantelides. Rehabilitation of cracked aluminium connections with GFRP composites for fatigue stresses. J Compos Construct ASCE 2007;11(3):328–335.
[15] A Fam, S Witt, S Rizkalla. Repair of damaged aluminum truss joints of highway overhead sign structures using FRP. Constr Build Mater 2006;20(10):948–956.
[16] X-L Zhao, L Zhang. State-of-the-art review on FRP strengthened steel structures. Eng Struct 2007;29:1808–1823.
[17] LL Hu, X-L Zhao, P Feng. Fatigue behavior of cracked high-strength steel plates strengthened by CFRP sheets. J Compos Constr 2016;20:4016043. doi:10.1061/(ASCE)CC.1943-5614.0000698.
[18] M Amraei, H Jiao, X-L Zhao, L-W Tong. Fatigue testing of butt-welded high strength square hollow sections strengthened with CFRP. Thin-Walled Struct 2017;120:260–268.
[19] H Jiao, X-L Zhao. CFRP strengthened butt-welded very high strength (VHS) circular steel tubes. Thin-Walled Struct 2004;42:963–978.
[20] C Miki, K Homma, T Tominaga. High strength and high performance steels and their use in bridge structures. J Constr Steel Res 2002;58:3–20.
[21] F Javidan, A Heidarpour, X-L Zhao, J Minkkinen. Application of high strength and ultra-high strength steel tubes in long hybrid compressive members: experimental and numerical investigation. Thin-Walled Struct 2016;102:273–285.
[22] S van Es, H Slot, H Senbergen, J Maljaars, R Pijpers. Use of HSS and VHSS in steel structures in civil and offshore engineering: requirements regarding material properties. Steel Construct 2018;11(4):249–256.
[23] M Amraei, A Ahola, S Afkhami, T Björk, A Heidarpour, X-L Zhao. Effects of heat input on the mechanical properties of butt-welded high and ultra-high strength steels. Eng Struct 2019;198:109460.
[24] M Amraei, M Dabiri, T Björk, T Skriko. Effects of workshop fabrication processes on the deformation capacity of S960 ultra-high strength steel. ASME J Manuf Sci Eng 2016;138(12). 121007-121007-13.
[25] S Fawzia, R Al-Mahaidi, X-L Zhao. Experimental and finite element analysis of a double strap joint between steel plates and normal modulus CFRP. Compos Struct 2006;75:156–162.
[26] AH Korayem, CY Li, QH Zhang, X-L Zhao, W-H Duan. Effect of carbon nanotube modified epoxy adhesive on CFRP-to-steel interface. Compos B 2015;79:95–104.
[27] S Fawzia, X-L Zhao, R Al-Mahaidi. Bond–slip models for double strap joints strengthened by CFRP. Compos Struct 2010;92:2137–2145.
[28] D Schnerch, M Dawood, S Rizkalla, E Sumner, K Stanford. Bond behavior of CFRP strengthened steel structures. Adv Struct Eng 2006. doi:10.1260/136943306779369464.
[29] C Wu, X-L Zhao, W-H Duan, R Al-Mahaidi. Bond characteristics between ultra high modulus CFRP laminates and steel. Thin-Walled Struct 2012;51:147–157.
[30] E Ghafoori, M Motavalli. Normal, high and ultra-high modulus carbon fiber-reinforced polymer laminates for bonded and un-bonded strengthening of steel beams. Mater Des 2015;67:232–243.
[31] Hart-Smith LJ. Adhesive-bonded double-lap joints. NASA-CR-112235; 1973.
[32] S Fawzia. Bond characteristics between steel and carbon fibre reinforced polymer (CFRP) composites PhD thesis. Melbourne: Civil Engineering Department, Monash University; 2007.
[33] LC Hollaway, J Cadei. Progress in the technique of upgrading metallic structures with advanced polymer composites. Prog Struct Mater Eng 2002;4:131–148.
[34] LS-DYNA Keyword User's Manual, Version R7.1, Livermore Software Technology Corporation (LSTC), Livermore, CA.
[35] M Amraei, T Skriko, T Björk, X-L Zhao. Plastic strain characteristics of butt-welded ultra-high strength steel (UHSS). Thin-Walled Struct 2016;109:227–241.
[36] Al-Emrani M, Linghoff D, Kliger R. Bonding strength and fracture mechanisms in composite steel-CFRP elements. In: Proceedings of the International Symposium on Bond Behaviour of FRP in Structures (BBFS 2005).

[37] P Colombi, C Poggi. Strengthening of tensile steel members and bolted joints using adhesively bonded CFRP plates. Constr Build Mater 2006;20:22–33.
[38] SH Xia, JG Teng. Behaviour of FRP-to-steel bonded joints. Proceedings of the international symposium BFS; 2005. p. 419–426.
[39] P Colombi, G Fava, L Sonzogni. Fatigue crack growth in CFRP-strengthened steel plates. Compos B 2015;72:87–96.
[40] AM Albat, DP Romilly. A direct linear-elastic analysis of double symmetric bonded joints and reinforcements. Compos Sci Technol 1999;59:1127–1137.
[41] T Yu, D Fernando, JG Teng, X-L Zhao. Experimental study on CFRP-to-steel bonded interfaces. Compos B 2012;43:2279–2289.